Structural Testing of 9 m Carbon Fiber Wind Turbine Research Blades*

Joshua Paquette†
Sandia National Laboratories‡, Albuquerque, NM, 87111

Jeroen van Dam§ and Scott Hughes§
*National Renewable Energy Laboratory**, Golden, CO, 80401*

Three 9 m carbon fiber wind turbine blades have been designed through a research program initiated by Sandia National Laboratories. The individual designs feature such innovations as carbon spar caps, material-induced twist-bend coupling, and flatback airfoils, among others. All blades were constructed with conventional dry lay-up and VARTM infusion processes. Static tests of these blades were conducted at the National Wind Technology Center. The blades were subjected to flapwise loading to simulate the extreme wind loads expected for each design in a Class 2b wind site. The blades were loaded with a three-point whiffle-tree arrangement. Upon obtaining the predetermined test load, the blades were subsequently loaded to failure. Load, deflection, strain, and acoustic emissions were monitored throughout the experiments. All blades survived the specified test loads, with two designs exceeding it significantly. In addition, carbon strains of over 0.8% in both tension and compression were recorded in one of the tests. Finally, acoustic microphones were able to detect areas where damage was occurring, and indicated the beginnings of failure. This paper outlines the results of the structural tests that were conducted.

Nomenclature

VARTM	=	Vacuum Assisted Resin Transfer Method
SNL	=	Sandia National Laboratories
NWTC	=	National Wind Technology Center
HP	=	High Pressure
LP	=	Low Pressure

I. Introduction

IN 2002, Sandia National Laboratories (SNL) initiated a research program[1] to demonstrate the use of carbon fiber in subscale blades[2] and to investigate advanced structural concepts through the Blade System Design Study (BSDS)[3,4,5]. From this effort, three 9 m designs were created by SNL with assistance from Global Energy Systems Consulting (GEC)††, Dynamic Design Engineering‡‡, and MDZ Consulting§§; and seven blades from each design were manufactured by TPI Composites***. All blades were designed for a 100 kW stall controlled turbine. The first blade set was called CX-100 (Carbon Experimental), and contained a full-length carbon spar cap, a relatively new concept at the time. The geometry of the CX-100 was based on the design of the ERS-100[6] blade at outboard span stations, and the Northern Power Systems NW-100 blade in the root area. The second blade design, the TX-100 (Twist-Bend Experimental), had the same geometry as the CX-100, but featured a significantly different laminate

† Wind Energy Technology Department, MS 1124
‡ Sandia is a multiprogram laboratory operated by Sandia Corporation, a Lockheed Martin company, for the U.S. Department of Energy under contract DE-AC04-94AL85000
§ National Wind Technology Center, MS3911
** NREL is operated by Midwest Research Institute, Battelle, Contract No. DE-AC36-99-GO10337
†† Global Energy Concepts, LLC, 5729 Lakeview Drive NE, Suite 100, Kirkland, WA 98033-7340, (425) 822-9008
‡‡ Dynamic Design Engineering, Inc., 123 C St., Davis CA, (530) 753-7961
§§ MDZ Consulting, 601 Clear Lake Road, Clear Lake Shores, Texas 77565, (281) 334-5681
*** TPI Composites, Inc., 373 Market Street, P.O. Box 328, Warren, RI 02885, (425) 247-1050

design. The blade was designed to have passive aerodynamic load reduction by orienting unidirectional carbon 20° off of the pitch axis in the skins from approximately 3.50 m outward. Studies[7,8,9,10,11,12] had indicated the possibility of such a method of passive aerodynamic load alleviation through material induced twist-bend coupling, with 20° being determined as the optimum angle. Other methods of twist-bend coupling have also been suggested[13,14,15,16]. The TX-100 also contained a fiberglass spar cap which terminated at the mid-span of the blade. The final blade design was named the BSDS, owing its name to the research program under which it was created. The BSDS had a length of 8.325 m rather than the 9.000 m length of the CX-100 and TX-100. This blade design exhibited a highly efficient structure which included such features as a thin, large-diameter root; flatback airfoils; integrated root studs; and a full-length, constant-thickness, carbon spar cap. A drawing of the plan form of these blades is shown in Figure 1, with the carbon-containing areas shown in blue. Note the carbon spar caps of the CX-100 and the BSDS blades, and the carbon outboard skins of the TX-100. The unidirectional fiberglass spar cap of the TX-100 is shown in red in the figure and extends only to the mid-span of the blade. It was determined that the large amount of carbon contained in the skin was adequate to carry loads outboard in this design, making a full length spar cap unnecessary. The narrow, constant thickness spar cap of the BSDS blade alludes to the inherent structural stiffness of this design. In addition, the BSDS design features a gradual transition between the root and max-chord areas as compared to the CX and TX plan form. Figure 2 provides a view of the two different blade geometries as seen from the trailing edge. Note the flat back on the inboard portion of the BSDS blade, as well as the larger root and smoother chord thickness transition.

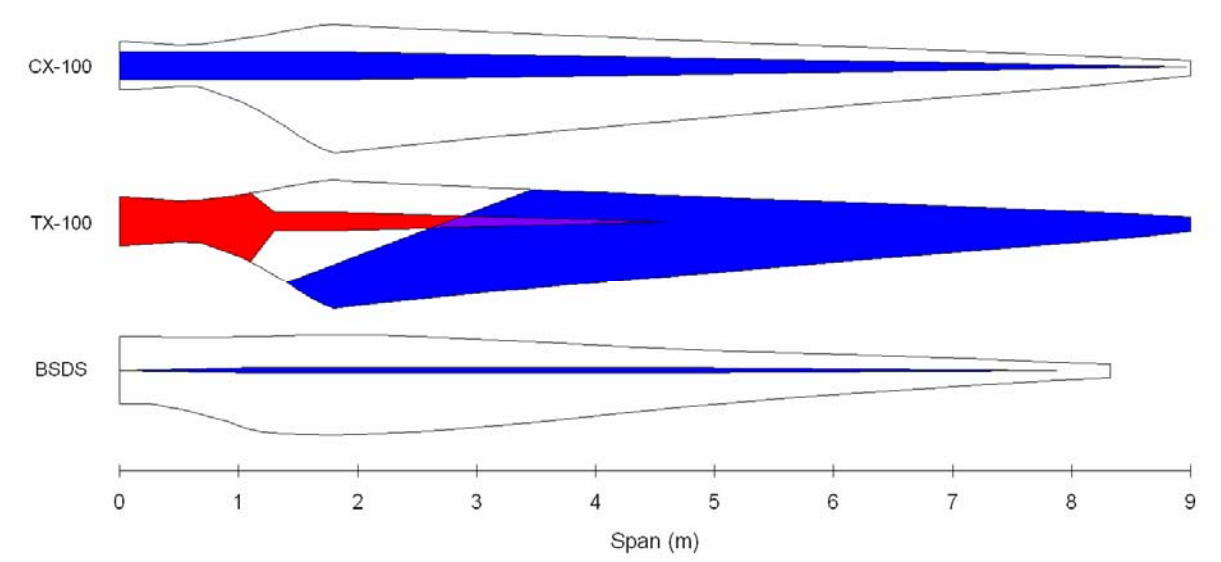

Figure 1: 9 m blade plan forms and major material regions.

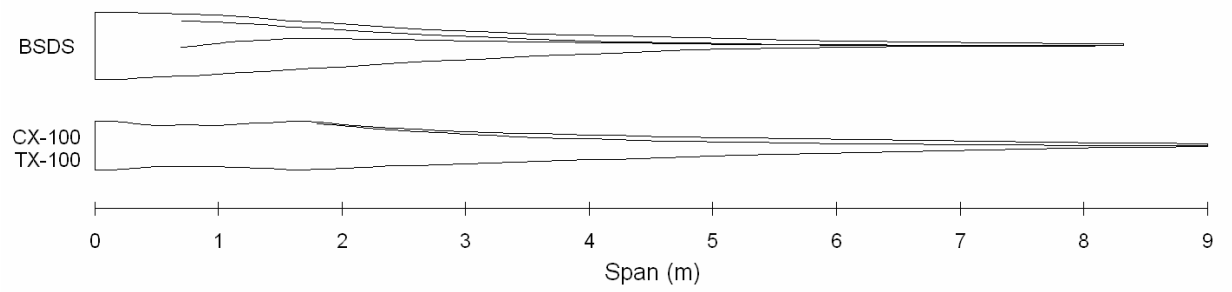

Figure 2: 9 m blade geometries as viewed from the trailing edge.

Figure 3 shows the airfoil geometries and relative sizes at the root, max-chord, and tip of the CX-100, TX-100, and BSDS blades. Note that in the figure the airfoils are shown without pre-twist. The BSDS blade can be seen to have a larger root diameter while also having a shorter max-chord length. The tip airfoil of the BSDS blade is representative of the outboard airfoils in the blade which are thin and aerodynamically high performing.

A suite of laboratory and field tests were proposed to verify that the manufactured blades met their design goals. In the laboratory, the blades were to undergo modal, static, and fatigue testing. To date, specimens from each design have undergone modal and static testing. This paper covers the results of the static testing.

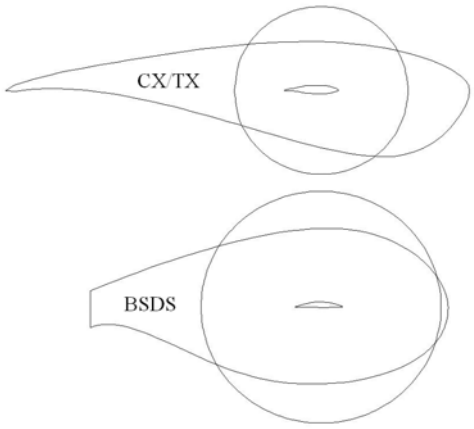

Figure 3: 9 m airfoil geometries at root, max-chord, and tip.

II. Test Setup

One blade from each design set was tested to failure at the National Wind Technology Center (NWTC) near Boulder, CO. In addition, a second TX-100 blade was tested to ascertain the effect that a manufacturing anomaly had on the blade. This anomaly was in the form of extra leading edge reinforcement material that was mistakenly added to the first four blades that were manufactured. This extra material was thought to have the potential to diminish the twist-bend coupling of the blades. TX-100 #004 contained the extra leading edge reinforcement and was tested to failure while the design specification TX-100 #007 was loaded to a representative proof load of 68% of the extreme load.

The blades were mounted to a 1360 kN-m test stand and subjected to a flapwise bending load case to approximate the extreme loading events for the wind class that each blade was designed to[17]. In the case of the CX-100 blade, the extreme load case resulted in a root moment of 86.4 kN-m. For the TX-100 and BSDS blades, the extreme load case resulted in a root moment of 53.8 kN-m. All blades were loaded by use of a three-point whiffle tree and saddle arrangement connected to an overhead bridge crane which is shown schematically in Figure 4.

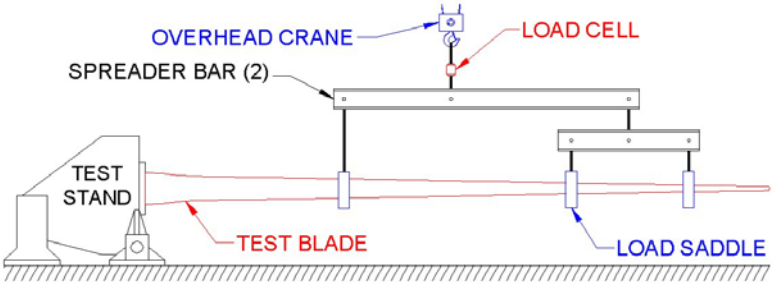

Figure 4: Three point whiffle-tree used in 9 m static blade tests.

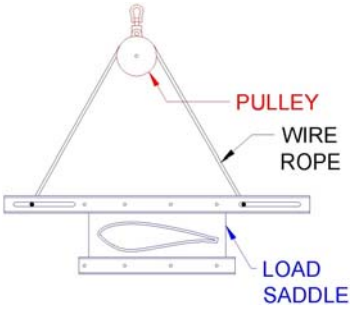

Figure 5: Rope and pulley arrangement for TX-100 blade test.

For the TX-100 blade test, a rope and pulley arrangement was attached to the saddles in an attempt to allow twisting without altering the loading point. When optimized correctly, the system can allow for loading through a stationary point on the chord line within a given rotation range. A schematic of the setup is shown in Figure 5.

A three-saddle whiffle-tree was also used for the BSDS blade test, but with different saddle stations. The saddle stations and applied loads at the 100% test load level are given for each blade in Table 1.

The blades were loaded and unloaded in increasing 25% increments up to the 100% test load as shown schematically in Figure 6. At each load step, the load was held for approximately 60 s. The 100% test load was calculated by multiplying the design load distribution for each blade by 1.10 to account for test-to-test variability. The resulting distribution was then approximated with a piece-wise linear fit achieved by point loads applied at the three saddle locations. The desired and applied test moment distributions for the CX-100, TX-100 and BSDS blade tests are shown in Figure 7, Figure 8, and Figure 9

Table 1: Saddle positions and loads* for 9 m static tests.

Saddle #	CX-100		TX-100		BSDS	
	Position (m)	Load (kN)	Position (m)	Load (kN)	Position (m)	Load (kN)
1	3.00	16.91	3.00	9.30	3.00	9.79
2	5.81	5.47	5.81	3.01	4.80	3.96
3	7.26	5.59	7.26	3.07	6.60	3.65

*Loads are for 100% test load

respectively. After reaching the 100% test load, loads were increased in 10% increments and held for 60 s until failure occurred (see Figure 6).

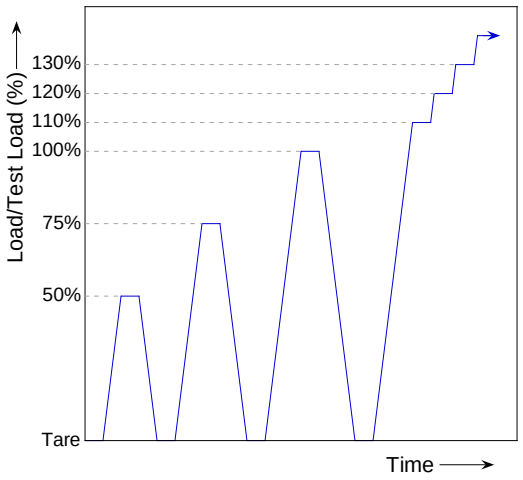

Figure 6: Loading sequence for 9 m blade tests.

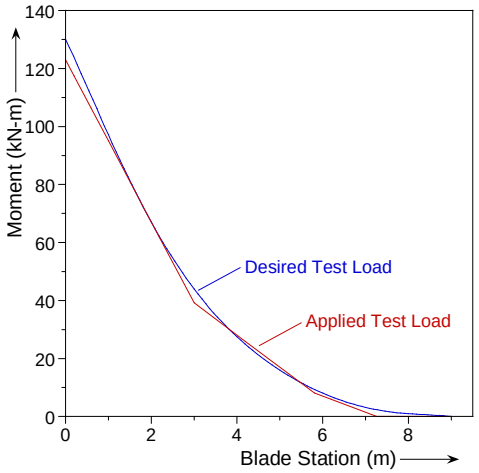

Figure 7: CX-100 test loading distribution.

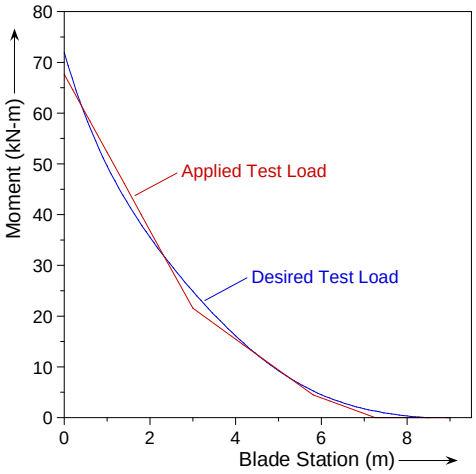

Figure 8: TX-100 test loading distribution.

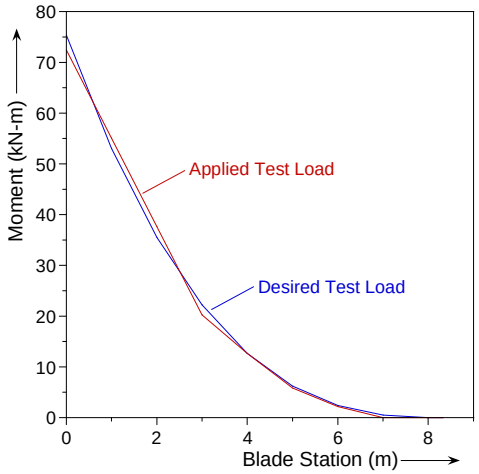

Figure 9: BSDS test loading distribution.

An array of sensors was used in the tests to monitor strain, deflection, load, and acoustic emissions. Load was monitored with a 100 kN load cell mounted between the whiffle-tree and the overhead crane (see Figure 4). Deflection was monitored by string potentiometers (pots) located near the saddle positions. For the CX-100 and BSDS blades, a string pot was located near the trailing edge of the blade near each saddle location. For the TX-100 test, additional string pots were mounted at the leading edge of the blade near the two inner most saddles to measure twist. Inclinometers were also mounted at 4.300 m and 6.250 m on the TX-100 blade to measure twist at those stations. The test blades were outfitted with a suite of 30-40 strain gages to measure strains along the blade centerline, in large panel regions near max-chord, and at other material and structural points of interest. Finally, the blades were instrumented with a grid of surface-mounted microphones to detect acoustic events that can point to regions of the blade incurring damage and thus, may indicate incipient failure regions.

III. Test Results and Analysis

All three blade designs successfully withstood the prescribed test loads. Figure 10 shows the maximum deflections that were measured in the three blade tests along with the corresponding root moments. The deflections are the result of a polynomial fit of the string pot results. The maximum tip deflections for the CX-100, TX-100, and BSDS blades were 1.05 m, 1.80 m, and 2.79 m respectively. Figure 11 compares the deflections at a root moment of 100 kN-m. The results show that the CX-100 blade was significantly stiffer than the TX-100 and BSDS blades.

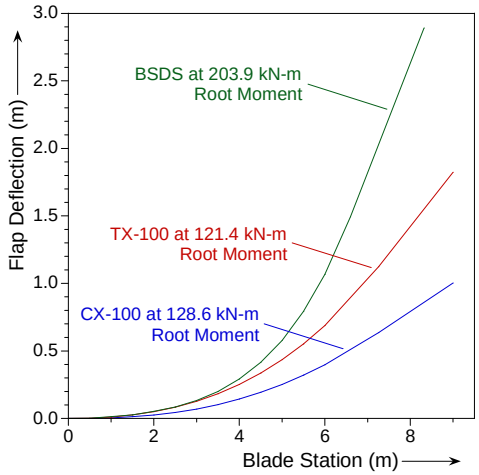

Figure 10: Maximum deflections for 9 m blades.

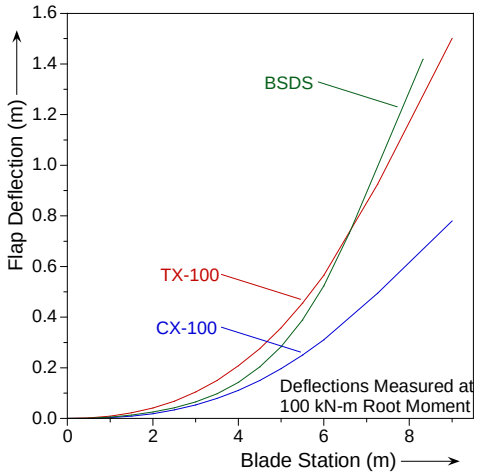

Figure 11: 9m blade deflections at 100 kN-m root moment.

The rotation angles about the spanwise axis at different stations of the TX-100 blade were measured during the test. The measurements were taken both from leading edge and trailing edge mounted string pots, and inclinometers mounted along the blade centerline. A positive angle corresponds to an increasing angle of attack for the airfoil at a given station. Figure 12 shows the twist angles that were measured at a 44.0 kN-m root moment in the test of blade #004 (blade with added material) and blade #007 (blade without added material) of the TX-100 blade set. Blade #004 was did not twist as much as blade #007 at the same load. This provides evidence of the effect that the extra leading material had on blade #004. Figure 13 shows the rotations measured along blade #004 at the 100% test load and at the failure load. The TX-100 blade showed a maximum twist of about -5° at the 6.25 m station for a root moment of 116.9 kN-m.

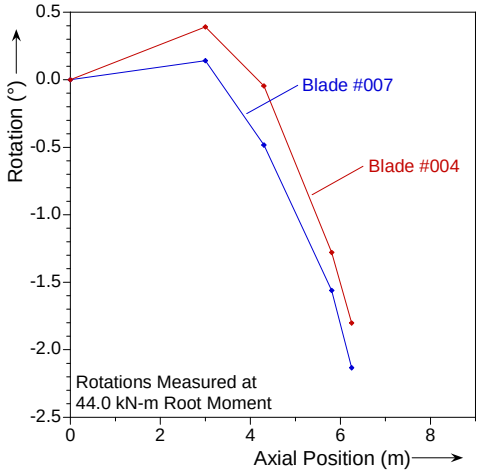

Figure 12: TX-100 #004 and #007 twist angles at 44 kN-m root moment.

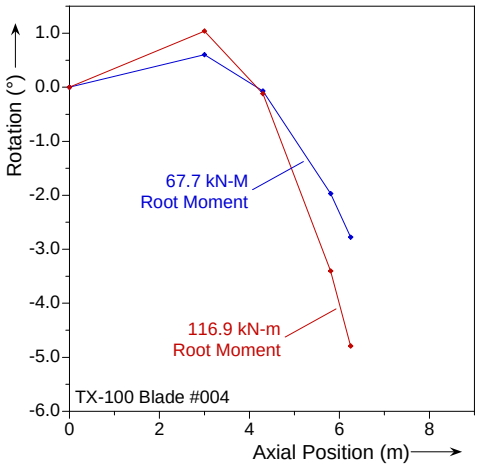

Figure 13: TX-100 #004 twist angle at test load and near failure.

Figure 14 shows the strains that were measured along the high-pressure and low-pressure spar caps for the three blades that were tested. Note that for the TX-100 blade, the spar cap terminates at the mid-span of the blade and thus strains outboard of that point are along the blade centerline. The carbon spar cap of the CX-100 blade experienced strains of around 3000 με before failure. The TX-100 blade exhibited maximum strains of approximately 5500 με near the termination point of the spar cap and strains elsewhere in the blade were generally lower. The high strain at the spar cap termination was likely the result of a stress concentration emanating from the tapered end of the spar cap (see Figure 1). The carbon spar cap of the BSDS blade experienced maximum strains of over 8000 με on both the high-pressure and low-pressure surfaces.

Figure 15, Figure 16, and Figure 17 show the strains measured in the panel regions aft of the spar cap for the CX-100, TX-100, and BSDS blades respectively. These are regions that are susceptible for buckling in extreme loading situations. The CX-100 and TX-100 blades showed indications of buckling in the 1.800 m region near a root moment of about 117 kN-m. These blades were of identical geometry and had similar construction in this area. Thus, this result is not unexpected. The BSDS blade showed slight signs of buckling at the 1.575 m station at around a 150 kN-m root moment. However, it is important to note that the blade continued to withstand load well beyond this point.

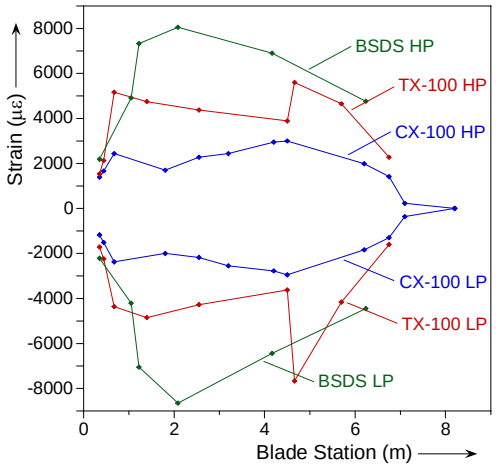

Figure 14: 9 m spar cap strains near failure.

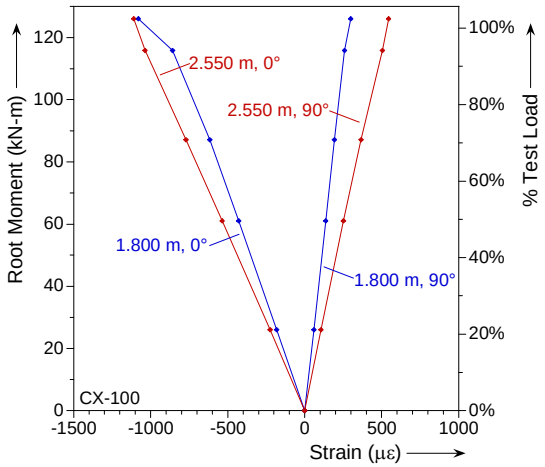

Figure 15: CX-100 aft panel strains parallel and perpendicular to blade axis.

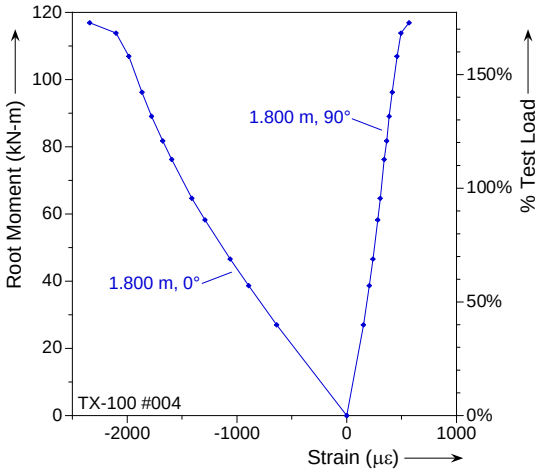

Figure 16: TX-100 aft panel strains parallel and perpendicular to blade axis.

For the BSDS test, strain gages were placed on the flat back, perpendicular to the blade axis at 0.580 m and at 1.575 m. The 0.580 m station contained one gage in the middle of the flatback (labeled 50%). At the 1.575-m station, gages were placed on the high pressure surface near the edge of the flat back (labeled 0%), on the low pressure surface near the flat back (labeled 100%), and at two intermediate positions, 25% and 75% of the distance between the high-pressure and low-pressure surfaces. The gages were intended to indicate if the flat back was collapsing or rotating relative to the high-pressure and low-pressure surfaces during the test. Figure 19 shows the strains measured at the aforementioned locations. Strain was linear with respect to load at the 0.580 m location, suggesting that the flat back was not buckling inward or outward at this location. All gages at the 1.575 m location show evidence of changes in the load path, especially beyond

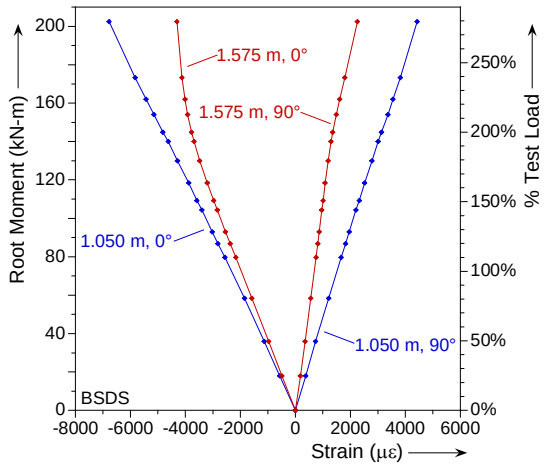

Figure 17: BSDS aft panel strains parallel and perpendicular to blade axis.

a root moment of 150 kN-m. The 0% and 25% gages start to change from compression to tension while the 75% and 100% gages exhibit an inflection in strain direction. This may suggest that the flat back was beginning to collapse by the low-pressure edge in a concave direction. The strains changing in opposite directions at the opposite ends of the flat back suggest that the flat back was not experiencing concave or convex panel buckling at the 1.575 m location.

Also of interest for the BSDS blade was the behavior of the root mounting studs. A novel root mounting stud design was implemented into the BSDS blade. The installation of the root mounting fasteners was integrated into the laminate infusion. Gages were placed near the tip of the most highly loaded root studs on the upper (low pressure) and lower (high pressure) surfaces. Gages were also placed at the same spanwise stations but between the root studs in the circumferential direction on the blade surface. Figure 18 shows the strain at these locations with respect to applied load. The resulting strains are relatively similar in magnitude and linear throughout the loading, indicating that the implementation of the root studs did not cause a significant stress concentration, with a relatively smooth load path between laminate and root stud. The root area was not observed to exhibit any signs of damage throughout testing.

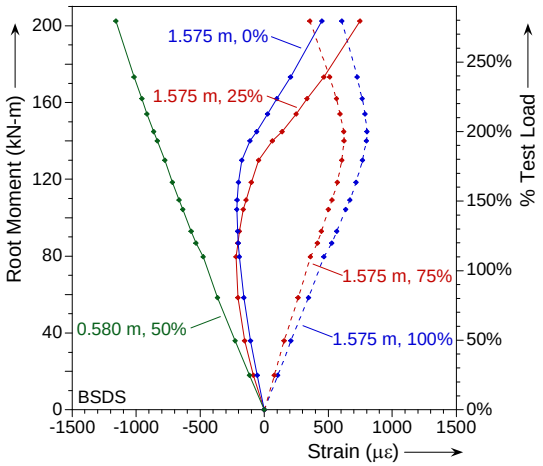

Figure 19: BSDS flat back strains.

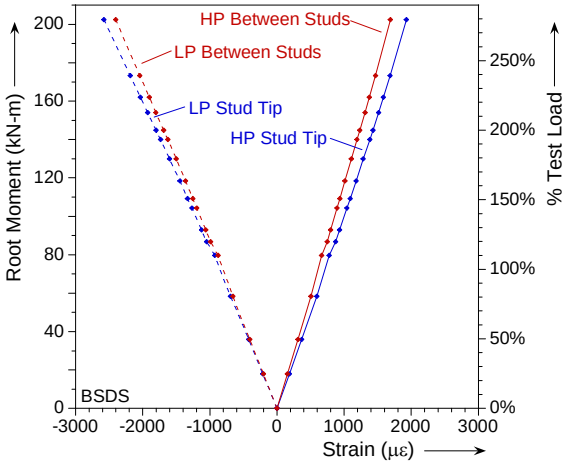

Figure 18: BSDS threaded rod strains.

The acoustic emissions sensed by microphones placed on the blade surface can be used to indicate the location of damage that the blade is incurring. This is accomplished by setting a time window in which individual microphones can detect the same event. The difference in time at which the event is detected by each microphone is used to triangulate the position on the surface that the microphones are mounted, assuming the velocity profile of the substrate is known. Unfortunately, the velocity profile is complicated in a composite structure which contains materials with widely varying acoustic transmission properties. The end result is a structure which has a velocity profile which is spatially and directionally dependent. For the results from these tests, various fits of the acoustic velocity field were used and were of the form

$$v = a + b\left(\left|\cos\alpha\right|\right)^n \tag{1}$$

where a, b, and n are fitting constants and α is the angle between the direction vector from the sensor to the event and the blade pitch axis. The resulting located events for the CX-100, TX-100, and BSDS blade tests are shown in Figure 20, Figure 21, and Figure 22 respectively. Each event is color coded with a respective energy range. It should be noted that this energy is not the true energy, as it represents the integral of the voltage vs. time curve. The true energy is defined by the integral of the voltage squared vs. time curve. These voltage vs. time results are useful for comparative

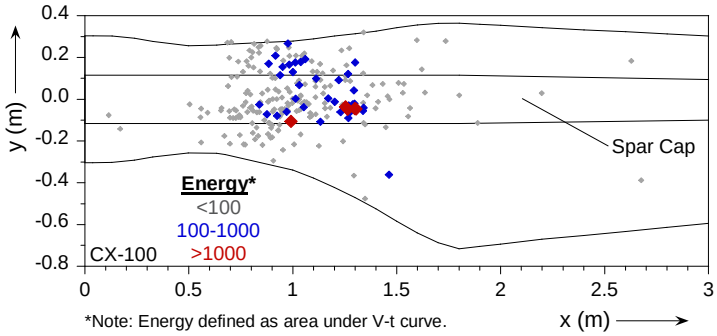

Figure 20: Acoustic event locations and energies for CX-100 blade test.

purposes however. The events are overlaid on outlines of each blade. Since the locations of the acoustic events are two-dimensional, the outlines are of the flattened low-pressure skins of the blades. In addition to the outlines of the blades, important regions such as spar caps and material boundaries are shown.

During the CX-100 test, several high-energy events were located between 1.20 m and 1.30 m along the spar cap. The CX-100 blade was observed during failure to experience a catastrophic buckling of the low-pressure skin near the 1.2-m station. A post mortem inspection of the blade in this region showed a large crack in the bond joint between the low pressure skin and the shear web. A photograph of the crack is shown in Figure 23.

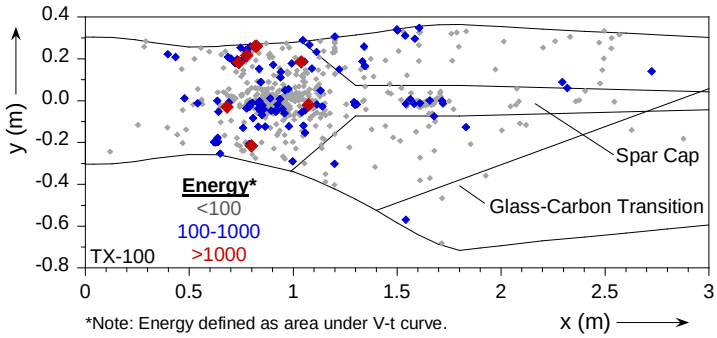

Figure 21: Acoustic event locations and energies for TX-100 blade test.

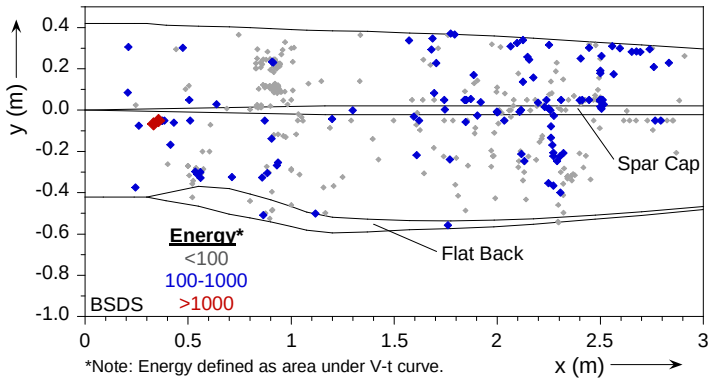

Figure 22: Acoustic event locations and energies for BSDS blade test.

Figure 23: Crack in shear web to LP skin bond joint at 1.20-1.30 m on the CX-100 blade.

The TX-100 blade test produced high-energy events just beyond the 1.00 m station. The blade eventually failed at the 1.0-m station, with a failure described as a buckling of the compressive skin, initiated towards the leading edge. A photograph of the fracture is shown in Figure 24.

During the BSDS test, the only high-energy events were located around 0.350 m, which the station where the shear web terminates on the root end. A closer examination of this area after the test showed that a large crack had developed between the low-pressure skin and the shear web in the bonding joint. A photograph of the crack is shown in Figure 25.

Figure 24: Crack near blade centerline on TX-100 blade.

Figure 25: Crack at shear web termination on the LP surface of the BSDS blade.

During the initial static test of the BSDS blade, the blade catastrophically failed near the 5.00 m station, with a root moment of 203.9 kN-m. The complete catastrophic failure at this station prohibited the assessment of the mode of failure. This is of interest as ostensibly panel buckling in the max airfoil stations of the blade was not the limiting factor in the static strength of the blade, as observed for other blades of this size. A second static strength test was performed on the BSDS in an attempt to obtain a failure in the inboard stations of the blade. A two-point whiffle tree was implemented to apply this load. During this second test, the blade failed near the 2.00 m station at a root bending moment of 220.2 kN-m.

In addition to indicating the location of damage occurring within a blade, acoustic emission monitoring is also a valuable tool for assessing when failure is occurring locally or globally. Figure 26, Figure 27, Figure 28, show the sum of the acoustic emission energy detected by all of the sensors in the root region of the CX-100, TX-100, and BSDS blades respectively. In each plot a trend line is drawn through the initial linear portions of the response. At some load, the response begins to become non-linear, indicating an acceleration of the acoustic emissions and the greater potential of failure. For the CX-100 and TX-100 blades, the acoustic emissions accelerate rapidly beyond root moments of 125 kN-m and 115 kN-m respectively. The response from the BSDS blade remained mostly linear until a root moment of 140 kN-m was reached. The accumulation of acoustic energy in the BSDS blade did grow non-linearly after 140 kN-m, although not as rapidly as for the other two blades.

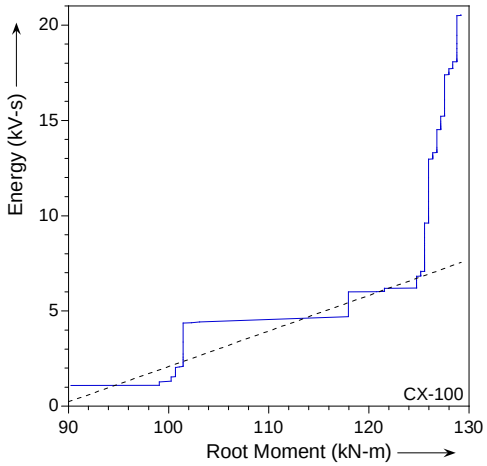

Figure 26: CX-100 acoustic energy accumulation.

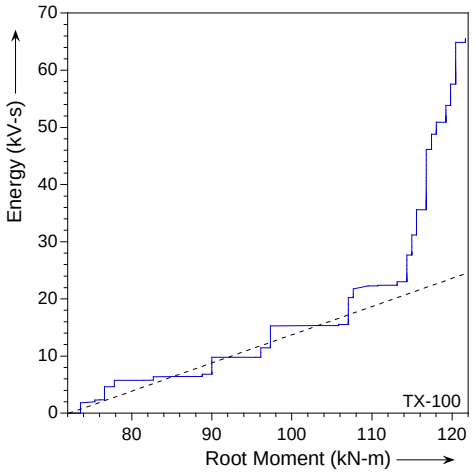

Figure 27: TX-100 acoustic energy accumulation.

A summary of salient results of the static tests of all three blade designs is contained in Table 2. The relatively high strength of the BSDS blade is evident, with the measured carbon strains approaching values seen in coupon testing of pre-preg specimens. This high strength combined with the significantly lower weight points to the structural advantages of this design in comparison to the CX-100 and TX-100.

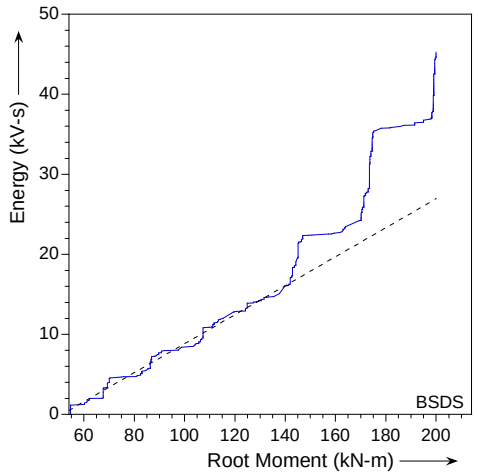

Figure 28: BSDS acoustic energy accumulation.

Table 2: Summary of results of 9 m blade tests.

Property	CX-100	TX-100	BSDS
Weight (lb)	383	361	289
% of Design Load at Failure	115%	197%	310%
Root Failure Moment (kN-m)	128.6	121.4	203.9
Max. Carbon Tensile Strain at Failure (%)	0.31%	0.59%	0.81%
Max. Carbon Compressive Strain at Failure (%)	0.30%	0.73%	0.87%
Maximum Tip Displacement (m)	1.05	1.80	2.79

IV. Conclusion

Specimens from three 9 m carbon fiber blade designs underwent static structural testing. All three test blades survived factored design test loading. The CX-100 blade displayed exceptional stiffness, deflecting only 1.05 m at a root moment of 128.6 kN-m. The blade failed due to panel buckling near max-chord which was likely initiated by a separation between the shear web and the low-pressure skin in that region. The TX-100 blade successfully demonstrated twist-bend coupling caused by 20° off-axis carbon in the outboard skins. The TX-100 blade failed at a slightly lower load than the CX-100 blade, but in a similar location. The BSDS blade displayed exceptional strength in comparison to the CX-100 and TX-100 designs, surviving to almost three times the target test load. The flat back airfoil feature performed well and did not display non-linear behavior until well after the target test load was reached. In addition, the root mounting studs of the BSDS blade were observed to have good static loading properties. Finally, the acoustic emission monitoring system detected not only the locations where damage was occurring, but also incipient global blade failure.

Acknowledgments

The authors would like to acknowledge Mark Rumsey, Perry Jones, and Wesley Johnson of SNL; Mike Jenks, Laura Rip, Dave Simms, and Walt Musial of NREL; Derek Berry of TPI Composites, Inc., Alan Beattie of PAC; Dayton Griffin of GEC; Kevin Jackson of Dynamic Design Engineering; and Mike Zuteck of MDZ Consulting for their assistance in the preparation and performance of these tests.

References

1 Ashwill, T, and Laird, D, “Concepts to Facilitate Very Large Blades,” Proceedings, ASME/AIAA Wind Energy Symposium, Reno, NV, 2007.

2 C.-H. Ong and S. W. Tsai, “The Use of Carbon Fibers in Wind Turbine Blade Design: A SERI-8 Blade Example,” SAND2000-0478, Sandia National Laboratories Contractor Report, March 2000.

3 Berry, Derek and Lockard, S., “Innovative Design Approaches for Large Wind Turbine Blades,” SAND2003-0723, Sandia National Laboratories, Albuquerque, NM, March 2003

4 Berry, Derek and Lockard, S., “Innovative Design Approaches for Large Wind Turbine Blades Final Report,” SAND2004-0074,Sandia National Laboratories, Albuquerque, NM, May 2004

5 Griffin, Dayton A., “Blade System Design Studies Volume II: Preliminary Blade Designs and Recommended Test Matrix,” SAND2004-0073, Sandia National Laboratories, Albuquerque, NM, June 2004

6 TPI Composites, Inc. Final Project Report, “Blade Manufacturing Improvements Development of the ERS-100 Blade,” SAND2001-1381, May 2001.

7 P. S. Veers, G. Bir and D. W. Lobitz, "Aeroelastic Tailoring in Wind-Turbine Blade Applications," Proceedings, Windpower '98 Meeting, pp. 291-304.

8 Lobitz, D. and Veers, P., “Aeroelastic Behavior of Twist-coupled HAWT Blades,” ASME/AIAA Wind Energy Symposium, Reno, NV, 1998, pp. 75-83.

9 Lobitz, D. and Laino, D., “Load Mitigation with Twist-coupled HAWT Blades,” ASME/AIAA Wind Energy Symposium, Reno, NV, 1999, pp. 124-134.

10 D. Lobitz, P. S. Veers and D. J. Laino, “Performance of Twist-Coupled Blades on Variable Speed Rotors,” Proceedings, ASME/AIAA Wind Energy Symposium, Reno, NV, 2000, pp. 404-412.

11 D. W. Lobitz et al., “The Use of Twist-Coupled Blades to Enhance the Performance of Horizontal Axis Wind Turbines,” SAND2001-1303, May 2001.

12 D. Griffin, “Evaluation of Design Concepts for Adaptive Wind Turbine Blades,” SAND2002-2424, Sandia National Laboratories Contractor Report, August 2002.

13 C-H Ong and S. W. Tsai, "Design, Manufacture and Testing of a Bend-Twist D-spar," Sandia National Laboratories Contractor Report, SAND99-1324, June 1999.

14 Wetzel, K., and Locke, J., “Uncoupled and Twist-bend Coupled Carbon-glass Blades for the LIST Turbine,” Proceedings, ASME/AIAA Wind Energy Symposium, Reno, NV, 2004, pp. 13-23.

15 Locke, James and Valencia, J., “Design Studies for Twist-Coupled Wind Turbine Blades,” SAND2004-0522, Sandia National Laboratories, Albuquerque, NM, June 2004

16 Wetzel, K., “Utility Scale Twist-Flap Coupled Blade Design,” Proceedings, ASME/AIAA Wind Energy Symposium, Reno, NV, 2005, pp. 382-394.

17 D. Berry, “Design of 9-meter Carbon-Fiberglass Prototype Blades Final Project Report,” SAND Report in preparation, Sandia National Laboratories, Albuquerque, NM, 2007